Article

Controlled Reduction of Vanadium Oxide Nanoscrolls: Crystal Structure, Morphology, and Electrical Properties

Serena A. Corr, Madeleine Grossman, Joshua D. Furman, Brent C. Melot, Anthony K. Cheetham, Kevin R. Heier, and Ram Seshadri

Chem. Mater., **2008**, 20 (20), 6396-6404 • DOI: 10.1021/cm801539f • Publication Date (Web): 24 September 2008

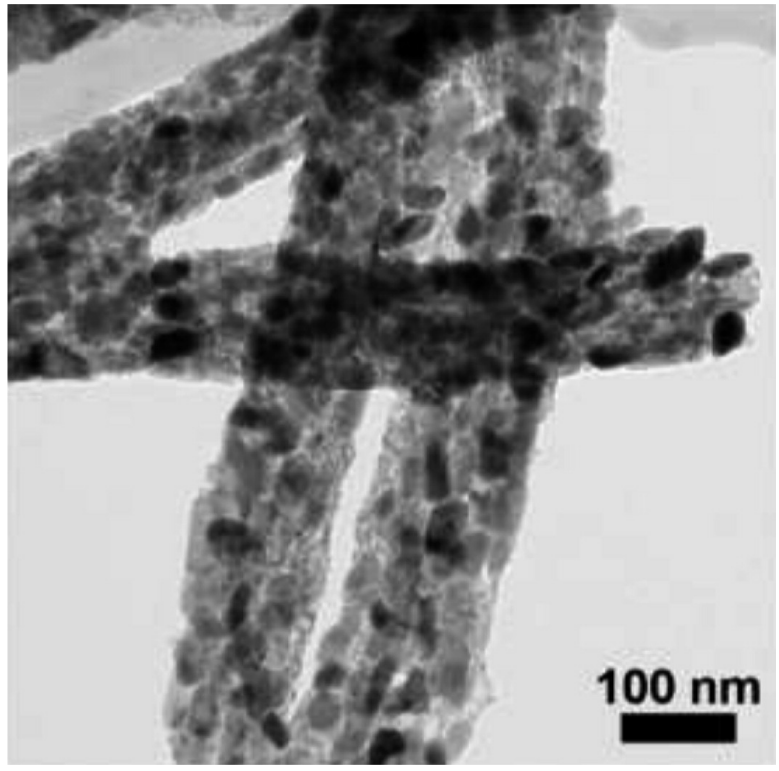

Controlled Reduction of Vanadium Oxide Nanoscrolls: Crystal Structure, Morphology, and Electrical Properties

Serena A. Corr,*,† Madeleine Grossman,† Joshua D. Furman,‡ Brent C. Melot,† Anthony K. Cheetham,‡ Kevin R. Heier,§ and Ram Seshadri†,||

Materials Department and Materials Research Laboratory, University of California, Santa Barbara, California 93106, Department of Materials Science and Metallurgy, University of Cambridge, United Kingdom CB2 3QZ, Department of Chemistry and Biochemistry, University of California, Santa Barbara, California 93106, and Air Products and Chemicals, Inc., Allentown, Pennsylvania 18195

Received June 6, 2008. Revised Manuscript Received August 6, 2008

The systematic and controlled reduction of vanadium oxide nanoscrolls results in routes to the large-scale preparation of nanostructures of the interesting and useful materials rutile VO_2 and corundum V_2O_3. Vanadium oxide ($V_2O_{5-\delta}$) nanoscrolls, prepared by the hydrothermal treatment of aged suspensions of V_2O_5 and dodecylamine, were reduced in a furnace in an atmosphere of 5% H_2:95% N_2 under different time and temperature conditions to monitor systematic trends in the structure and morphology of the resulting oxides. The products were characterized by X-ray diffraction (XRD), electron microscopy, N_2 sorption measurements, and electrical transport studies. We find that the reduction conditions (time and temperature) play a significant role in determining the crystal structure and morphology of the products. At short times and low temperatures, the reduction products are rutile VO_2. These convert to corundum V_2O_3 when temperatures are increased. In all cases, the appearance of crystalline Bragg peaks in XRD is associated with the breaking up of the starting high-aspect nanostructures into small, dense crystallites. Under certain reduction conditions, porous materials with ill-defined X-ray structures are obtained as intermediates.

Introduction

Vanadium oxides are a rich and diverse family of compounds with several applications. Vanadium dioxide (VO_2) undergoes a well-documented transition from a semiconductor to a metal at ~340 K, accompanied by a structural change.[1] Above this temperature, VO_2 adopts the tetragonal rutile structure and is metallic.[2] Below the transition temperature, VO_2 is monoclinic, because of the pairing of V atoms (Figure 1), and this is associated with semiconducting behavior, with a band gap of ~0.7 eV. The resistivity of VO_2 in its metallic state is in the range of 2×10^{-4} to 5×10^{-4} Ω cm^3 and displays a sudden and large increase when cooled below the transition temperature. Changes in electrical properties drive large changes in optical properties between the low- and high-temperature phases; the low-temperature monoclinic structure is somewhat infrared (IR)-transparent, whereas the tetragonal phase is opaque.

V_2O_3 also undergoes a metal-to-insulator transition, albeit at a lower temperature (~150 K). In this case, the low-temperature insulating, antiferromagnetic phase adopts a monoclinic structure, with a conversion to a paramagnetic, metallic corundum structure observed above 150 K.[1,4−6] Again, a large change in electrical resistivity—approximately 6 orders of magnitude—is observed.[1] These reversible structural transitions, with their associated large electrical property changes, make VO_2 and V_2O_3 very attractive candidates for a wide variety of technological applications,

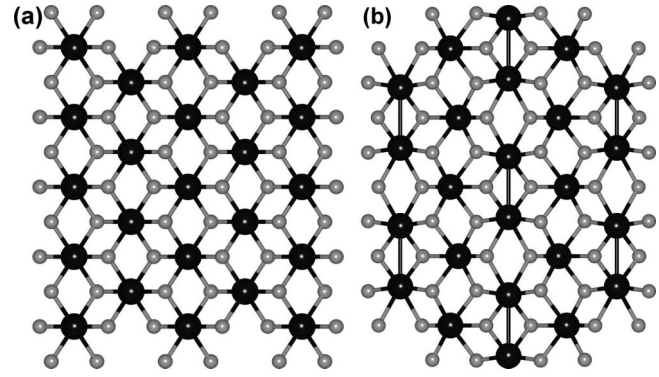

Figure 1. Structure of (a) the high-temperature tetragonal rutile form of VO_2 and (b) the low-temperature monoclinic form, showing alternating short (indicated by bonds) and long V−V distances. The large dark spheres are vanadium atoms and the small lighter spheres are oxygen atoms.

* Author to whom correspondence should be addressed. Fax: 805 893 8797. E-mail address: serena@mrl.ucsb.edu.
† Materials Department and Materials Research Laboratory, University of California.
‡ Department of Materials Science and Metallurgy, University of Cambridge.
§ Air Products and Chemicals, Inc.
|| Department of Chemistry and Biochemistry, University of California.

(1) Morin, F. J. *Phys. Rev. Lett.* **1959**, *3*, 34–36.
(2) Zylbersztejn, A.; Mott, N. F. *Phys. Rev. B* **1975**, *11*, 4383–4395.
(3) Berglund, C. N.; Guggenheim, H. J. *Phys. Rev.* **1969**, *185*, 1022–1033.
(4) Frenkel, A. I.; Stern, E. A.; Chudnovsky, F. A. *Solid State Commun.* **1997**, *102*, 637–641.
(5) Isaacs, E. D.; Platzman, P. M.; Metcalf, P.; Honig, J. M. *Phys. Rev. Lett.* **1996**, *76*, 4211–4214.
(6) Qazilbash, M. M.; Schafgans, A. A.; Burch, K. S.; Yun, S. J.; Chae, B. G.; Kim, B. J.; Kim, H. T.; Basov, D. N. *Phys. Rev. B* **2008**, *77*, 115121-1–115121-10.

10.1021/cm801539f CCC: $40.75
Published on Web 09/24/2008

Chart 1. 3 × 3 Matrix Showing the Conditions under Which the Reduction Experiments Were Carried Out in 5% H_2:95% N_2

1 h	3 h	6 h	
A	B	C	400 °C
D	E	F	500 °C
G	H	J	600 °C

including use in optical switching devices[7,8] and field effect transistors.[9] Oxides of vanadium are also frequently used as catalysts in many reactions.[10]

Recently, several groups have reported routes to nanostructures of these and other reduced vanadium oxides. A common preparative procedure for nanostructured vanadium oxide materials involves the hydrothermal treatment of a vanadium precursor (e.g., NH_4VO_3, vanadium alkoxides, V_2O_5, or $VOSO_4$).[11−14] Nesper and co-workers have reported the use of alkyl amines as structural templating agents for the preparation of VO_x nanoscrolls from vanadium alkoxides.[15] Cross-sectional transmission electron microscopy (TEM) images confirmed the scroll-like nature of these nanocomposites, where the amine molecules act as intercalants between successive vanadium oxide sheets. Further structural details of these materials have recently been elucidated using the pair-distribution function approach.[16] A simpler route to nanoscroll production has been reported by Mai et al., who used V_2O_5 as a precursor material to yield gram quantities of product.[17] Aromatic amines with increasing chain lengths have also been used as reducing agents to selectively provide nanoneedles, nanorods, and nanotubes.[18] Li et al. have also used a reducing agent (specifically oxalic acid) to tune their final product morphology; they reported the formation of nanobelts, olive-shaped VO_2 nanostructures, and petal-shaped nanostructures with increasing concentrations of the reducing agent.[19] Sun et al.[20] have examined the electrochemical and intercalative properties of VO_x nanoscrolls. VO_2 nanowires prepared via the hydrothermal treatment of NH_4VO_3, followed by pyrolysis and reduction, have also been reported.[14] In the case of vanadium sesquioxide (V_2O_3), nanocrystals with an average size of 20−50 nm have been prepared using benzyl alcohol and vanadium(V) isopropoxide.[21]

Here, we report a systematic study of the effect of reduction on vanadium oxide nanoscrolls. The ensuing nanostructures are either X-ray-amorphous, crystalline rutile VO_2 or corundum V_2O_3, and, under certain conditions, combinations of some of the above. The starting nanoscrolls and the products of reduction have been characterized by X-ray diffraction (XRD), scanning electron microscopy (SEM), TEM, and nitrogen (N_2) sorption measurements. Some of the reduced samples of VO_2 and V_2O_3 have been pressed into pellets and studied via temperature-dependent four-probe electrical resistivity measurements. Reduction conditions (time and temperature) significantly influence the crystal structure, porosity, morphology, and properties of the product materials. At short reduction times and at relatively low reduction temperatures, the products are rutile VO_2. These convert to corundum V_2O_3 when reduction temperatures are increased, interestingly going through phases that are almost X-ray amorphous. The appearance of crystalline Bragg peaks in XRD, which are associated with rutile VO_2 and/or corundum V_2O_3, is signaled in TEM analysis by the breakup of the initial high-aspect-ratio nanostructures into small dense crystallites. Transport studies on pressed pellets of VO_2 and V_2O_3 nanostructures suggest that the electrical behavior, including the phase transition temperatures, are similar to the properties measured on bulk or thin-film samples.

Experimental Section

Dodecylamine (1.88 g; 0.01 mol) was dissolved in ethanol (15 cm^3). Vanadium(V) oxide (1.81 g; 0.01 mol) in 15 cm^3 of deionized water was added dropwise to the stirred amine solution. The mixture was allowed to undergo stirring at room temperature for 3 days, after which it was hydrothermally treated for 48 h at 180 °C. After cooling to room temperature, the resulting dark gray powder was washed with water, ethanol, and diethyl ether to remove any unreacted amine. The powders were dried overnight at 70 °C in a vacuum oven. The powders (henceforth referenced as original nanoscroll samples) were characterized by XRD, SEM, and TEM. The sample was then divided into nine parts and reduced in 5% H_2:95% N_2. The reduction reactions were performed according to the conditions presented in Chart 1. Initial studies showed that porous nanotubes were observed to form at 500 °C; therefore, we conducted a set of experiments above and below this temperature to better understand and explore their formation. We also investigated the effect of reduction time on the end product. The various reduced powder samples were characterized by XRD, SEM, TEM and N_2 sorption measurements. Several of the reduced samples were pressed into pellets and studied using electrical transport measurements.

XRD patterns were obtained using a Philips X Pert Pro X-ray diffractometer with Cu Kα radiation (1.5418 Å) at a 45 kV accelerating voltage and 40 mA. Powder patterns were analyzed

(7) Soltani, M.; Chaker, M.; Haddad, E.; Kruzelesky, R. *Meas. Sci. Technol.* **2006**, *17*, 1052–1056.
(8) Eguchi, R.; Tsuda, S.; Kiss, T.; Chainani, A.; Muraoka, Y.; Hiroi, Z.; Shin, S. *Phys. Rev. B* **2007**, *75*, 073102-1–073102-4.
(9) Kim, H.-T.; Chae, B.-G.; Youn, D.-H.; Maeng, S.-L.; Kim, G.; Kang, K.-Y.; Lim, Y.-S. *New J. Phys.* **2004**, *6*, 52-1–52-19.
(10) Greenwood, N. N.; Earnshaw, A. *Chemistry of the Elements*, 2nd Edition; Butterworth−Heinemann: Boston, 2004.
(11) Chen, X.; Sun, X.; Li, Y. *Inorg. Chem.* **2002**, *41*, 4524–4530.
(12) Liu, J.; Li, Q.; Wang, T.; Yu, D.; Li, Y. *Angew. Chem., Int. Ed.* **2004**, *43*, 5048–5052.
(13) Pavasupree, S.; Suzuki, Y.; Kitiyanan, A.; Pivsa-Art, S.; Yoshikawa, S. *J. Solid-State Chem.* **2005**, *178*, 2152–2158.
(14) Kam, K. C.; Cheetham, A. K. *Mater. Res. Bull.* **2006**, *41*, 1015–1021.
(15) Muhr, H.-J.; Krumeich, F.; Schönholzer, U. P.; Bieri, F.; Niederberger, M.; Gauckler, L. J.; Nesper, R. *Adv. Mater.* **2000**, *12*, 231–234.
(16) Petkov, V.; Zavalij, P. Y.; Lutta, S.; Whittingham, M. S.; Parvanov, V.; Shastri, S. *Phys. Rev. B* **2004**, *69*, 085410-1–085410-6.
(17) Mai, L.; Chen, W.; Xu, Q.; Zhu, Q.; Han, C.; Peng, J. *Solid State Commun.* **2003**, *126*, 541–543.
(18) Sediri, F.; Gharbi, N. *J. Phys. Chem. Solids* **2007**, *68*, 1821–1829.
(19) Li, G.; Chao, K.; Peng, H.; Chen, K.; Zhang, Z. *Inorg. Chem.* **2007**, *46*, 5787–5790.
(20) Sun, D.; Kwon, C. W.; Baure, G.; Richman, E.; MacLean, J.; Dunn, B.; Tolbert, S. H. *Adv. Funct. Mater.* **2004**, *14*, 1197–1204.
(21) Pinna, N.; Antonietti, M.; Niederberger, M. *Colloid Surf. A* **2004**, *250*, 211–213.

using the Rietveld method as embodied in the Rietveld code.[22] In situ thermodiffractometry was performed on a Bruker D8 Advance diffractometer fitted with an Anton Parr platinum high-temperature stage. Samples were measured in air in 5 K increments from 303 K to 393 K, with a step size of 0.0145°. The powder sample was mixed with ethanol to form a thick slurry, which was deposited dropwise onto the platinum stage and allowed to dry. SEM images were acquired on a FEI XL30 Sirion FEG digital scanning microscope. Samples were deposited directly on an aluminum stub, using a double-sided adhesive carbon tape. TEM images were acquired using a FEI Tecnai G2 Sphera microscope. Samples for TEM were prepared by dispersion in ethanol for 10 min in an ultrasonic bath. A drop of the sample was deposited on a lacey carbon coated copper grid and allowed to dry before imaging.

BET surface areas were determined on a Micrometrics Tristar 3000 sorption analyzer using a low-temperature N_2 adsorption method. The analysis gas used was N_2, and liquid nitrogen was used as the cryogen. Samples were dried and degassed by heating to 90 °C for 1 h and then 150 °C for 3 h under a N_2 environment. Isotherm raw data were collected by evacuating and then cooling the samples to liquid nitrogen temperature and exposing them to the analysis gas at a series of precisely controlled pressures. The Barrett−Joyner−Halenda (BJH)[23] method was applied for pore size distribution analysis, using the Micrometrics software package.

Electrical property measurements were conducted using a Quantum Design Physical Properties Measurement System (PPMS). Four-probe resistivity measurements were conducted on pressed pellets of the samples. Electrical contacts were established using silver epoxy. To press pellets, a force of 2×10^3 kg was applied over a bar-shaped pellet with an area of 1.35 cm × 0.7 cm.

Results and Discussion

$V_2O_{5-\delta}$ Nanoscrolls. The lamellar structure of V_2O_5 facilitates a mechanism whereupon the amine-intercalated slabs roll up under hydrothermal treatment.[11] In this process, the amine surfactant molecules accumulate and condense between the vanadate layers. Upon heating, this results in more-ordered structures, with the lamellar sheets finally rolling into nanotube structures. The final black material is a result of the partial reduction of some V^{5+} to V^{4+} by amine decomposition.[24]

Xie and co-workers previously noted that the hydrothermal treatment times play a role in the resulting morphology of nanoscrolls.[25] These authors prepared vanadium oxide nanobelts via the hydrothermal treatment of V_2O_5 and sodium dodecylsulfate. They have found that hydrothermal treatment times had an effect on the aspect ratio of the nanobelts, with an increase noted at longer reaction periods. They also noted a morphology dependence on temperature, with a mixture of belts and particles obtained at lower temperatures. We performed a series of experiments to determine the optimum hydrothermal treatment times and found that the highest-aspect-ratio nanoscrolls were obtained after 2 days. Experiments that were conducted for 3, 8, and 14 days experienced the evolution of shorter nanoscrolls, with the formation of spherical agglomerates for the two-week reaction.

The scroll-like morphology of the products of the two-day hydrothermal treatment of the dodecylamine-intercalated V_2O_5 has been confirmed by TEM and SEM (see Figures 2a−d). The TEM images indicate that the nanoscrolls are typically composed of 20 layers. The average interlayer spacings are determined to be 2 nm, in agreement with previously reported results (see Figure 2b). This is contrary to the larger spacings reported for the materials obtained by the hydrothermal treatment of vanadium alkoxide in the presence of hexadecylamine, where spacings near 3 nm were reported.[26,27] Here, the inner tube dimensions are 30 nm, whereas the average scroll width is 110 nm. The average thickness of the scrolls from SEM is 120 nm. There is a slight difference, in comparison to the TEM values, which is due to the gold coating of the SEM sample. SEM images show the shortest nanoscrolls (~2 μm), whereas the longest typically stretch to 5 μm in length (see Figures 2c and d).

XRD data collected of the original nanoscrolls shows broad, symmetric 00*l* reflections with *d* spacings near 10 and 7 Å, which are consistent with the 002 and 003 reflections, (see Figure 3a). The rather large widths of these peaks are consistent with the very thin nanoscroll walls. These peaks are symmetric and Lorentzian when plotted in terms of the 2θ angle. The peaks at higher angles for the intralayer *hk*0 *d*-spacings attest to the crystalline nature of the nanoscrolls. These peaks correspond to the 200, 210, and 310 reflections. The peaks display an asymmetric sawtooth profile, which suggests that there is a registry mismatch (turbostratic disorder) between the layers (see Figure 3b). In agreement with the interpretation of turbostratic disorder, no general *hkl* reflections are found.

Reduction of the Nanoscrolls. The reduction experiments were performed on the nanoscrolls according to the conditions presented in Chart 1. Samples were placed in an alumina crucible in a tube furnace under flowing 5% H_2: 95% N_2. The heating rate for each experiment was set at 5 °C/min.

X-ray patterns for all reductions are shown in Figure 4. The X-ray pattern of sample A corresponds to monoclinic rutile VO_2. Increasing the reduction time to 3 h (sample B) or to 6 h (sample C) maintains the monoclinic rutile VO_2 structure. When the reduction is performed at 500 °C for 1 h (sample D), rutile VO_2 remains the predominant phase. At this temperature, as the reduction duration is increased, the monoclinic rutile VO_2 begins to convert to corundum V_2O_3. For the intermediate reduction time of 3 h (sample E), the overall peak intensity decreases and the pattern can be fit to a mixture of monoclinic rutile VO_2 and corundum V_2O_3 by Rietveld analysis (data not shown here). It is possible that the overall intensity of the XRD pattern decreases (sample E), as a result of the oxygen sublattices of rutile and corundum being quite different in their

(22) Bérar, J.-F.; Baldinozzi, G. *J. Appl. Crystallogr.* **1993**, *26*, 128–129.
(23) Barrett, E. P.; Joyner, L. G.; Halenda, P. P. *J. Am. Chem. Soc.* **1951**, *73*, 373–380.
(24) Chandrappa, G. T.; Steunou, N.; Cassaignon, S.; Bauvais, C.; Livage, J. *Catal. Today* **2003**, *78*, 85–89.
(25) Shi, S.; Cao, M.; He, X.; Xie, H. *Cryst. Growth Des.* **2007**, *7*, 1893–1897.
(26) Spahr, M. E.; Bitterli, P.; Nesper, R.; Müller, M.; Krumeich, F.; Nissen, H. U. *Angew. Chem., Int. Ed.* **1998**, *37*, 1263–1265.
(27) Spahr, M. E.; Stoschitzki-Bitterli, P.; Nesper, R.; Haas, O.; Novák, P. *J. Electrochem. Soc.* **1999**, *146*, 2780–2783.

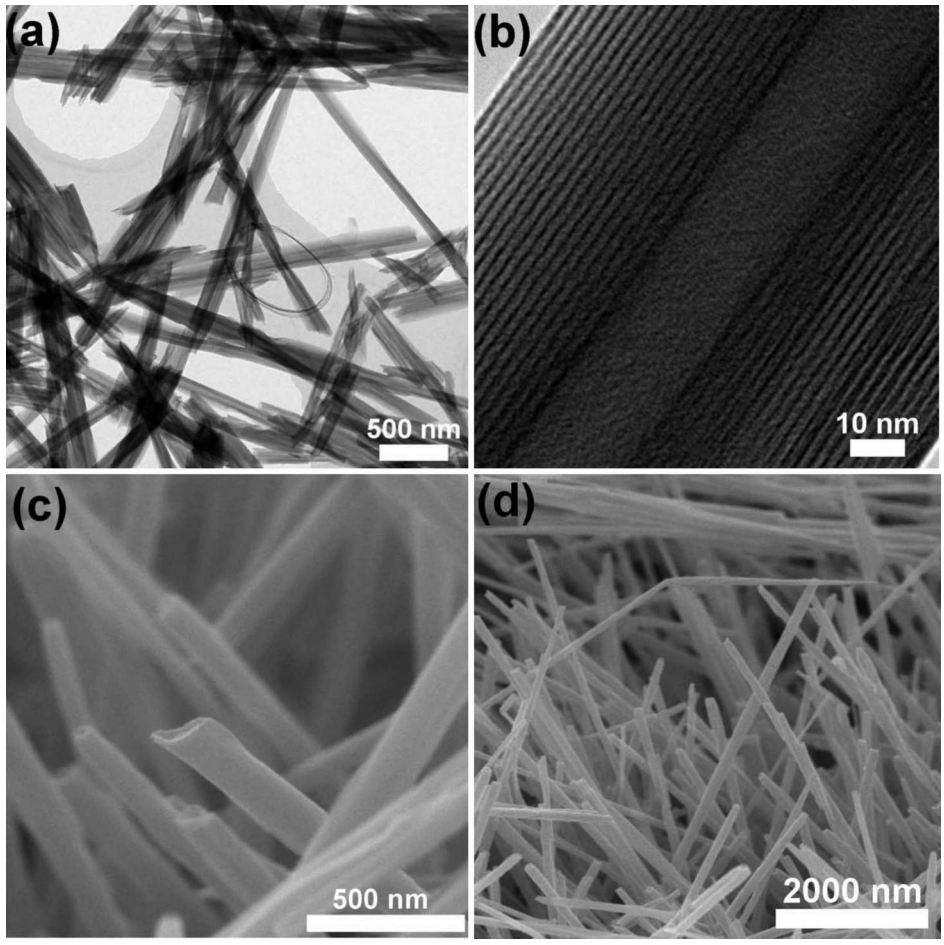

Figure 2. (a, b) TEM and (c, d) SEM images of hydrothermally prepared $V_2O_{5-\delta}$ nanoscrolls prepared for two days. The average diameter of the nanoscrolls is 125 nm, whereas the average length stretches several micrometers long (typically 5 μm). Regular interlayer spacings of ~2 nm are evident from higher-magnification TEM images, and there are typically 20 layers per scroll.

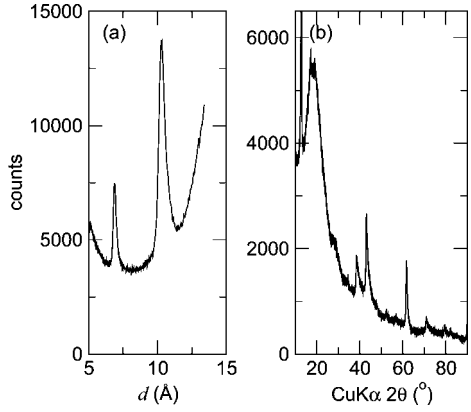

Figure 3. XRD patterns of the nanoscrolls showing (a) the symmetrical Lorentzian reflections at large *d*-spacings, which is consistent with 003 and 002 reflections (for $c \approx 20$ Å), and (b) the higher-angle reflections beyond 20° 2θ, which display the sawtooth profiles associated with *hk*0 correlations that are typical of a lamellar system with poor registry between layers. Note the large hump near $2\theta \approx 20°$, which suggests the presence of amorphous components.

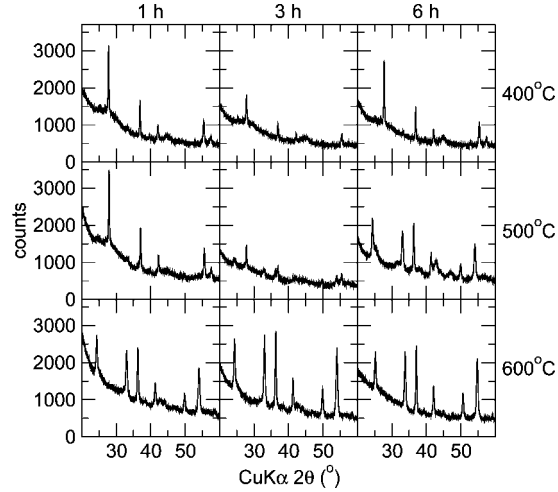

Figure 4. XRD patterns following the 3 × 3 matrix shown in Chart 1. For the highest temperatures, the predominant phase is corundum V_2O_3, while rutile VO_2 is the preferred phase at lower temperatures. None of the samples show any evidence of the starting nanoscrolls. Samples prepared at 500 °C, depending on the duration of the reduction, are rutile VO_2 (sample D, 1 h) or corundum V_2O_3 (sample F, 6 h), with a mixture of both phases evident in sample E (3 h). All samples reduced at 600 °C are corundum V_2O_3 (samples G, H, J).

topologies, which requires the conversion to be accompanied by extensive bond breaking and remaking. An increase in the 500 °C reduction time to 6 h results in a sample that is predominantly V_2O_3 (sample F). For all samples prepared at 600 °C (samples G−J), irrespective of the reduction time, the predominant phase is corundum V_2O_3. Particle sizes were calculated using the line widths from Rietveld refinements and the Scherrer equation. Curiously, Scherrer analysis suggested that all the VO_2 samples (samples A−D) were in the size range of 31−37 nm, whereas all the V_2O_3 samples

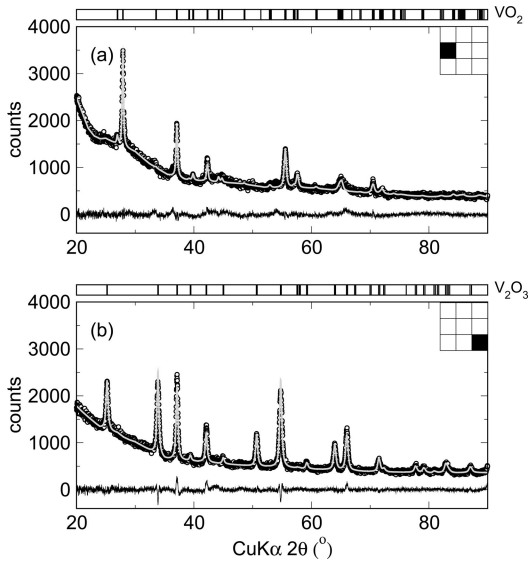

Figure 5. Observed (open circles) and calculated (gray line) X-ray diffraction (XRD) patterns for samples prepared at 500 °C for 1 h (sample D) and at 600 °C for 6 h (sample J). The bottom trace in each frame is the difference pattern on the same scale. The reduction conditions (from Chart 1) are indicated schematically in each panel.

Table 1. Specific Surface Area and Average Pore Size from BET Measurements for the Different Reduced Samples

sample	specific surface area (m^2/g)	average pore size (nm)
A	33	41
B	26	>100
C	31	66
D	44	45
E	73	22
F	77	39
G	73	15
H	75	15
J	66	15

(samples E−J) were in the range of 25−28 nm, regardless of the heating temperature or time.

All the XRD patterns were analyzed by Rietveld refinement, as a means of establishing phase purity and sample quality. We show these patterns for samples reduced at 500 °C for 1 h (sample D) and at 600 °C for 6 h (sample J) in Figure 5. Sample D was fit to monoclinic rutile VO_2 in space group $P12_1/c1$, with a resulting R_w value of 4.86%. Sample J was fit to the corundum structure of V_2O_3 in space group $R\bar{3}CH$ with a resulting R_w value of 4.58%. In these samples, no other crystalline phases were discerned. From the results of the Rietveld refinements, we confirm that the structures were almost indistinguishable, in terms of cell parameters and cell volume from the reported bulk structures of rutile VO_2[28] or corundum V_2O_3.[29]

The SEM images of the reduced samples (Figure 6) suggest that the overall morphology of the starting scrolls is maintained, albeit with a shrinkage of the diameter. When the reduced objects are seen end-on, one can see that the objects are tubular and, in this discussion, will be referenced as nanotubes. The diameter generally decreases as the reduction time increased from 1 h to 6 h for samples. For example, when the reduction time increased from 1 h to 3 h for samples reduced at 400 °C (samples A−C), a decrease in diameter from 100 nm to 90 nm is noted. This decrease in diameter is also observed in TEM images (see Figure 7). In the case of samples prepared at 400 °C, the average tube diameter after 1 h reduction (sample A) is 106 nm, and this diameter decreases to 87 nm after 6 h of reduction (sample C). As the temperature is increased to 600 °C, there is a large spread in the average length of the nanotubes. Figure 6 shows sample J (bottom right), where populations of smaller and longer tubes are evident. Samples reduced for 6 h both at 500 °C (sample F) and at 600 °C (sample J) show a roughening of the surface of the tubes, because of the formation of facetted crystallites.

There is a distinct difference in the morphology of the reduced nanotubes, when compared with the parent nanoscroll sample, as observed from the TEM images (see Figure 7). As a general rule, all the samples seem somewhat porous by TEM. As the extent of reduction (time, temperature) increases, the porous objects develop second phases of small, denser particles, which we associate with crystalline VO_2 or V_2O_3. Samples A, B, and C (which were reduced at 400 °C) do not show any of these dense particles, although the XRD patterns do suggest the presence of rutile VO_2. The pattern of sample B, in conjunction with the nature of the TEM images, suggests that the porous tissue-like materials are almost X-ray amorphous. There is a noted decrease in the number of the dense crystalline objects in sample E, consistent with XRD patterns for this material, which show a decrease in overall intensity. When the time is increased to 6 h (sample F), there is a return of crystalline material (almost all corundum V_2O_3, as seen via XRD), with an average size of 23 nm, calculated from TEM images. For all samples prepared at 600 °C (samples G, H, J) V_2O_3 nanocrystals with an average size of 24 nm are noted, which is in close agreement with the Scherrer analysis.

To summarize the structural and morphological information, we can conclude that the nanocrystals present in sample D are rutile VO_2, whereas those present in samples F, G, H, and J are corundum V_2O_3. The observed decrease in the average diameter for all reduced samples, compared to the original nanoscrolls, is presumably due to the loss of the amine template during the reduction process. To confirm this presumption, we performed thermogravimetric analysis (TGA) of the original nanoscrolls and the reduced samples. TGA of the original nanoscrolls shows an initial mass loss between 220 and 260 °C of 2.5%, with a 32.9% mass loss noted up to 470 °C, which was due to the loss of the amine intercalant. This is in close agreement with previous studies, where dodecylamine was used as a template for the preparation of TiO_2 frameworks.[30] In the case of the reduced samples, there is a decrease in the mass of the material lost due to the removal of the amine template during the reduction step. For sample A (prepared at 400 °C for 1 h), there is a total mass loss of 9.0%, whereas in the case of sample G (prepared at 600 °C for 1 h), this mass loss is even smaller

(28) McWhan, D. B.; Marezio, M.; Remeika, J. P.; Dernier, P. D. *Phys. Rev. B* **1974**, *10*, 490–495.
(29) Vincent, M. G.; Yvon, K.; Ashkenazi, J. *Acta Crystallogr., Sect. A: Cryst. Phys., Diffr., Theor. Gen. Crystallogr.* **1980**, *36*, 808–813.
(30) Wang, Y.; Ma, C.; Sun, X.; Li, H. *J. Non-Cryst. Solids* **2003**, *319*, 109–116.

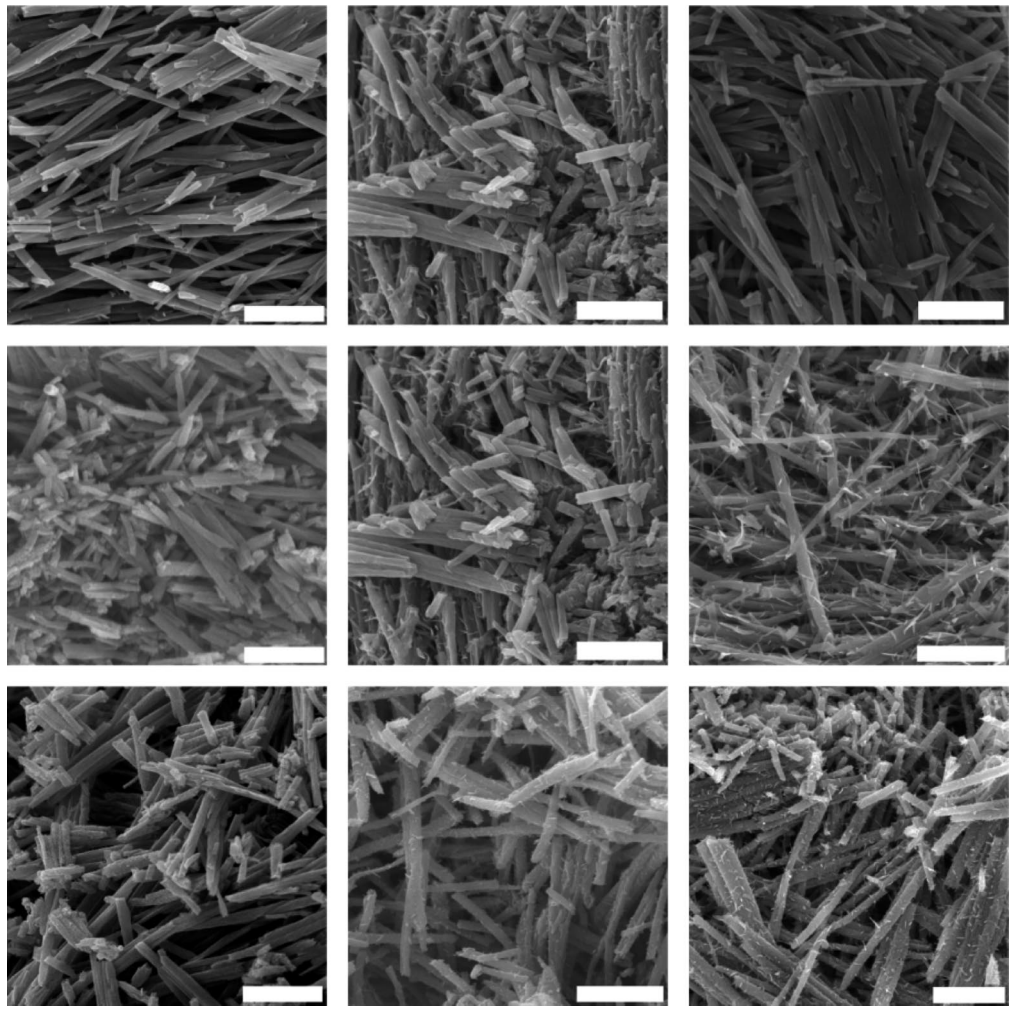

Figure 6. SEM images of reduced samples, following the 3 × 3 matrix described in Chart 1. The scale bar in each image is 1 μm.

(4.9%). These observations are consistent with the assertion from electron microscopy studies that the shrinkage in diameter of our reduced samples, compared to the original nanoscrolls, is due to the loss of amine intercalant. All the samples contain a porous, almost-X-ray amorphous component with diaphanous morphology.

N_2 adsorption and desorption isotherms were obtained for the reduced nanotube samples to determine the average pore diameter and surface area (Figure 8). The presence of a hysteresis for each sample is indicative of a type IV isotherm, which is characteristic for materials with average pore sizes of 2−50 nm.[31,32] Surface area measurements and average pore diameters are detailed in Table 1. There is a clear trend of increasing surface area with increasing temperature noted from porosimetry measurements. The surface area scales approximately inversely with the average pore size obtained from Barrett−Joyner−Halenda (BJH) analysis[23] of the sorption data. The initial large pores, which result in materials with small surface areas, occur because the intercalated amines play the role of sacrificial pore formers. As these are calcined, the volume loss that accompanies the reduction of V_2O_5 to reduced species provides a further source of porosity in the reduced materials, in a manner similar to what has been observed in materials such as $ZnMn_2O_4$[33,34] and Mn_3O_4.[35] This final stage of pore formation due to reduction, and oxygen loss yields materials with mesoscopic pores and large surface areas. As the reduction treatment time is increased, there is initially a greater loss of amine, resulting in the formation of a more porous structure. The largest surface areas determined here are found when reduction conditions are set at 500 °C for 6 h (sample F, 77 m^2/g). All the samples heated at 600 °C display surface areas that decrease as the reduction time increases, suggesting a balance between driving off the organic material, the opening of pores due to vanadium reduction, and the closure of pores due to sintering. Previous work by Pavasupree et al. on VO_2 nanorod samples prepared by the hydrothermal treatment of laurylamine hydrochloride, vanadium alkoxide, and acetylacetone have been reported to have surface areas near 40 m^2/g.[13]

(31) Brunauer, S.; Emmett, P. H.; Teller, E. *J. Am. Chem. Soc.* **1938**, *60*, 309–319.
(32) Brunauer, S.; Deming, L. S.; Deming, W. E.; Teller, E. *J. Am. Chem. Soc.* **1940**, *62*, 1723–1732.
(33) Toberer, E. S.; Seshadri, R. *Adv. Mater.* **2005**, *17*, 2244–2246.
(34) Toberer, E. S.; Löfvander, J.; Seshadri, R. *Chem. Mater.* **2006**, *18*, 1047–1052.
(35) Toberer, E. S.; Schladt, T. D.; Seshadri, R. *J. Am. Chem. Soc.* **2006**, *128*, 1462–1463.

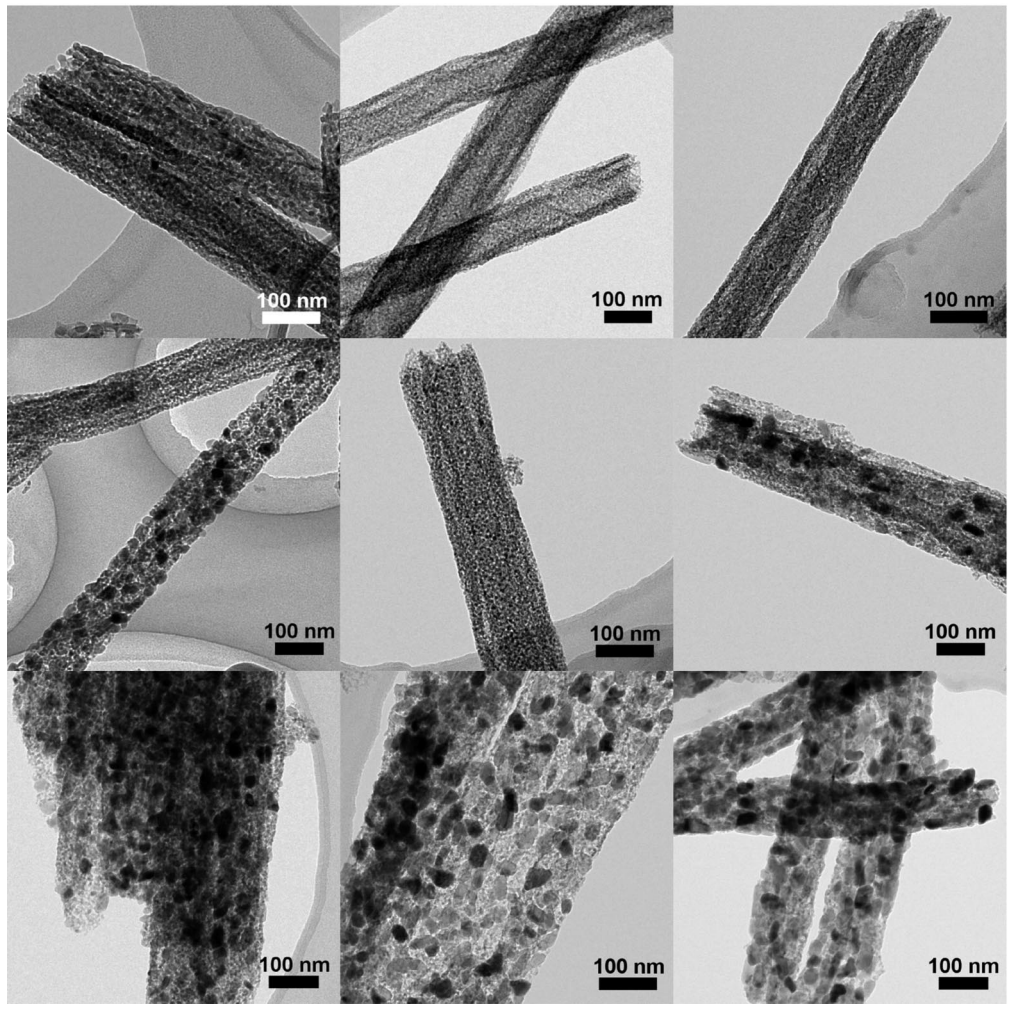

Figure 7. TEM images of reduced samples, following the 3 × 3 matrix described in Chart 1. The porosity of the tubes is evident from the images, along with an increase in the presence of crystalline material, as we move to higher temperatures.

Properties of the Product Oxides. Thermodiffractometry was performed on sample D (rutile VO_2) to monitor the structural change from monoclinic to tetragonal upon heating (see Figure 9). A diffraction pattern was collected after every 5 K change in temperature, from 303 K to 393 K. A shift in the peaks at 27.8° and 36.9° 2θ is evident from Figure 9a upon heating through the transition temperature. To follow the somewhat subtle change across the phase transition, two-phase Rietveld refinements were performed on each pattern, using the *tetragonal* structure of VO_2 as one of the phases, and face-centered cubic platinum (fcc-Pt) (the heating stage) as the other. The unit-cell volume of tetragonal VO_2, which is twice the average volume per VO_2 formula unit, from the refinements is plotted as a function of temperature in Figure 9b. The transition is characterized by a sudden increase in the average volume per VO_2 formula unit, with a maximum being reached just slightly beyond 340 K, near 350 K following which a small decrease in the volume (0.09%) is observed until the temperature reached 360 K. Following this, there is almost no change in the cell volume until 390 K. Changes in the unit-cell volume over the metal−insulator transition temperature have been previously reported by several groups.[36−38] In Figure 9b, we compare results from two prior studies on single crystals, neither of which suggest the small decrease that we see. It is possible that this small region with negative thermal expansion is a property of the nanocrystalline nature of the VO_2. Negative thermal expansion is not unusual in compounds at temperatures just above the structural transition, and this is observed, for example, in $PbTiO_3$.[39]

Temperature-dependent DC electrical resistance measurements were performed on pressed pellets of samples A (predominantly VO_2), D (VO_2), and H (V_2O_3). The data are respectively displayed in the three panels of Figure 10. Because the pellets were not sintered, one should note that the magnitudes of the resistances reported here provide an upper bound and the true resistance values of the grains are likely to be lower. The first-order insulator-to-metal transition in VO_2 is observed here, centered at 340 K with a 20 K thermal hysteresis, similar to numerous earlier reports, where the lack of an abrupt change in resistivity was attributed to oxygen nonstoichiometry.[40,41] Previous reports also show a decrease in the resistivity of pressed pellet samples of VO_2 as the temperature rises above 340 K, rather than true metallic

(36) Minomura, S.; Nagasaki, H. *J. Phys. Soc. Jpn.* **1964**, *19*, 131–132.
(37) Kucharczyk, D.; Niklewski, T. *J. Appl. Crystallogr.* **1979**, *12*, 370–373.
(38) Rao, K. V. K.; Naidu, S. V. N.; Iyengar, L. *J. Phys. Soc. Jpn.* **1967**, *23*, 1380–1382.
(39) Megaw, H. D. *Ferroelectricity in Crystals*; Methuen: London, 1957.

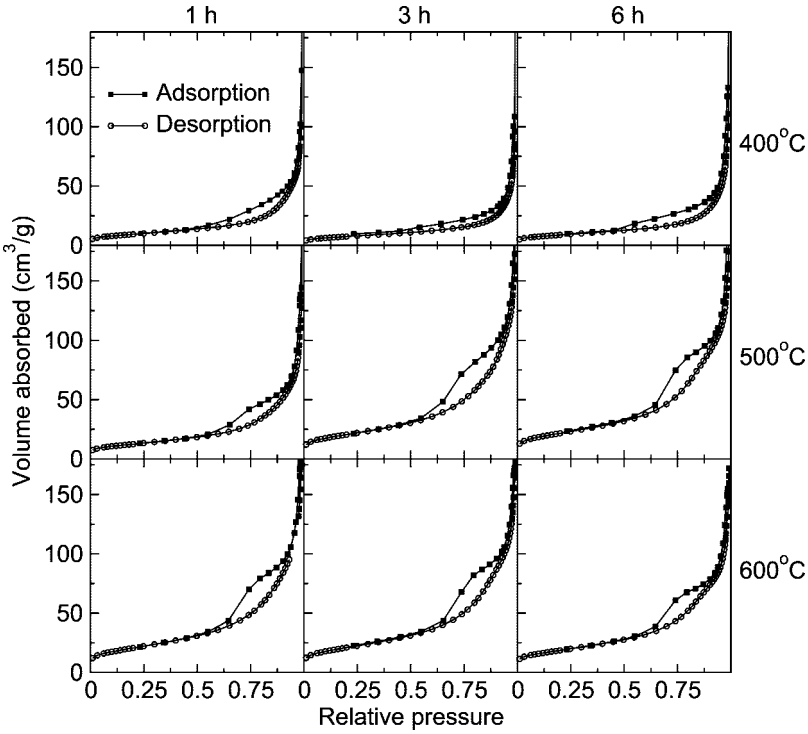

Figure 8. N_2 sorption isotherms at 77 K for reduced samples, following the 3 × 3 matrix from Chart 1. The hysteresis between the data obtained when the pressure is increased (labeled adsorption) and decreased (labeled desorption) indicates the presence of mesoporosity.

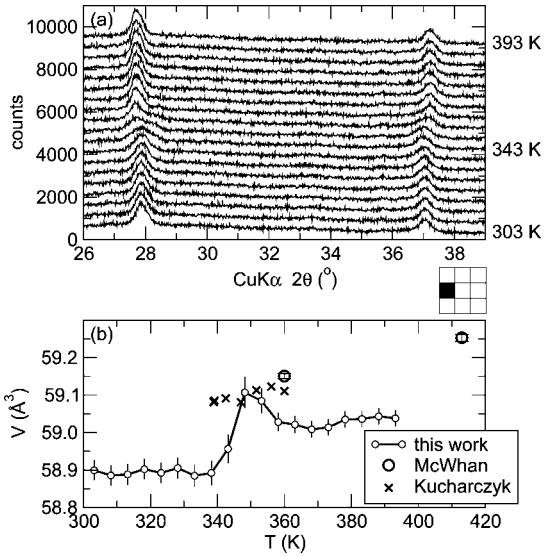

Figure 9. (a) Thermodiffractometry of the reduced VO_2 nanotubes (sample D) upon heating from 303 K to 393 K in increments of 5 K; note a shift to the left of the peak at 27.8° 2θ when the temperature is increased. (b) Monoclinic-to-tetragonal phase transition in VO_2 monitored using changes in the refined tetragonal unit-cell volume, as a function of increasing temperature. Data taken on single-crystal VO_2 samples, as reported by McWhan et al.[28] and Kucharczyk and Niklewski.[37]

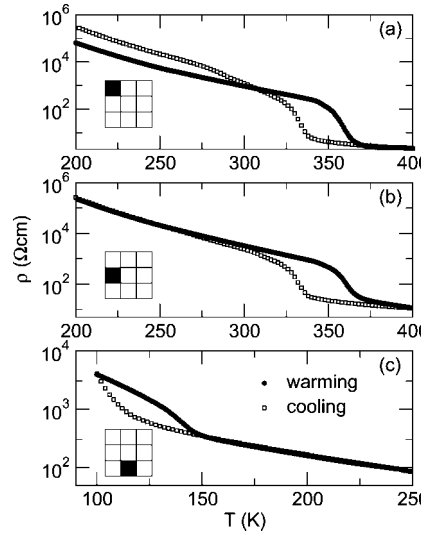

Figure 10. Resistivity as a function of temperature acquired upon warming and cooling, for reduced samples prepared at (a) VO_2, 400 °C, 1 h; (b) VO_2, 500 °C, 1 h; and (c) V_2O_3, 600 °C, 3 h.

behavior.[42,43] For example, in a study of powder and thin-film VO_2, Guinneton et al. have found an order-of-magnitude increase in the resistivity of their films, compared to a pressed pellet of particulate material.[44] It has been suggested that the absence of a true metallic state, in terms of a positive temperature coefficient of resistance, can result because of grain boundaries.[43,45] For sample A, we note that the resistivity near room temperature is on the order of tens of Ω cm. Upon warming from the lowest temperature (limited by the measured resistance value, exceeding 10^6 Ω), the resistivity decreases and a hysteresis effect is noted, with a ΔT value of ∼24 K. The large decrease in resistivity at ∼340 K (taking the midpoint of the hysteresis) is indicative of a phase transition. In the case of sample D, the hysteresis again centers at 340 K, as expected for a samples of VO_2, with a ΔT value of ∼28 K.

The V_2O_3 sample (sample H) is a better conductor at room temperature, with resistivity on the order of hundreds of mΩ cm. Again, upon cooling, the predominant behavior is semiconducting. The narrower hysteresis ($\Delta T \approx 19$ K) is centered at ∼120 K, which is lower than the expected phase-transition temperature ($T_{I-M} \approx 150$ K).

Conclusions

Careful consideration of the experimental design provides a convenient route to rutile VO_2 and corundum V_2O_3 via the reduction of amine-templated $V_2O_{5-\delta}$ nanoscrolls. Reduction time and temperature have a significant effect on the morphology and structure of the vanadium oxide nanowires that are obtained. One interesting morphological feature of these materials is their porosity, in combination with the presence of nanocrystalline material. The evolution of crystallites of rutile VO_2 and corundum V_2O_3 can be tracked using XRD, where the observed intensities increase as the temperatures increase. The effect of the reduction treatment times is most evident in samples prepared at 500 °C. At 500 °C, a 1 h reduction yields rutile VO_2, whereas a 6 h reduction gives corundum V_2O_3. There is a marked increase in X-ray peaks corresponding to corundum V_2O_3 in all samples prepared at 600 °C, with crystalline material noted in all TEM images. Both experimental factors that have been studied have effects on the resulting products. Lower temperatures yield rutile VO_2 nanotubes—the phase confirmed by Rietveld analysis—which display room-temperature resistivity values on the order of tens of Ω cm. The metal-to-insulator transition temperatures for both VO_2 samples measured (samples A and D) occur at 340 K. The metal-to-insulator transition for the V_2O_3 sample (sample H) shows a shift to lower transition temperature (120 K), compared to the values for single crystals from the literature (150 K).[1] The structural transition from the low-temperature insulating phase to the high-temperature metallic, tetragonal structure has also been monitored here, using thermodiffractometry. We anticipate that the new nanostructures could find many potential applications as new inexpensive conducting or switchable materials.

Acknowledgment. This work was supported by funding from Air Products & Chemicals, Inc. Further support from the UC Discovery program, and from the National Science Foundation (Career Award No. DMR 0449354) and the use of MRSEC facilities (through No. DMR 0520415) is acknowledged.

CM801539F

(40) Goodenough, J. B. *Phys. Rev.* **1960**, *117*, 1442–1451.
(41) Wu, X.; Tao, Y.; Dong, L.; Wang, Z.; Hu, Z. *Mater. Res. Bull.* **2005**, *40*, 315–321.
(42) Ningyi, Y.; Jinhua, L.; Chenglu, L. *Appl. Surf. Sci.* **2002**, *191*, 176–180.
(43) Li, J.; Yuan, N. *Appl. Surf. Sci.* **2004**, *233*, 252–257.
(44) Guinneton, F.; Sauques, L.; Valmalette, J. C.; Cros, F.; Gavarri, J. R. *J. Phys. Chem. Solids* **2001**, *62*, 1229–1238.
(45) Gentle, A.; Maaroof, A.; Smith, G. *Curr. Appl. Phys.* **2008**, *8*, 229–232.